

Article

Charge Transfer on the Surface-Enhanced Raman Scattering of Ag/4-MBA/PEDOT:PSS System: Intermolecular Hydrogen Bonding

Yuenan Pan ¹, Wei Wang ¹, Shuang Guo ², Sila Jin ², Eungyeong Park ², Yantao Sun ^{1,*}, Lei Chen ^{1,*} 
and Young Mee Jung ^{2,*} 

¹ College of Chemistry, Jilin Normal University, Siping 136000, China; panyuenan0219@163.com (Y.P.); 18043657873@139.com (W.W.)

² Department of Chemistry, Institute for Molecular Science and Fusion Technology, Kangwon National University, Chunchon 24341, Korea; guoshuang@kangwon.ac.kr (S.G.); jsira@kangwon.ac.kr (S.J.); egpark@kangwon.ac.kr (E.P.)

* Correspondence: 15504341819@163.com (Y.S.); chenlei@jlnu.edu.cn (L.C.); ymjung@kangwon.ac.kr (Y.M.J.); Tel.: +82-33-250-8495 (Y.M.J.)

Abstract: A sandwich-structured noble metal-probe molecule-organic semiconductor consisting of Ag nanoparticles (NPs), 4-mercaptobenzoic acid (4-MBA) and different concentrations of poly(styrenesulfonate:poly(3,4-ethylenedioxythiophene) (PEDOT:PSS) was prepared by layer-by-layer assembly. Intermolecular hydrogen bonding was observed to have a significant effect on the surface-enhanced Raman scattering (SERS) of Ag/4-MBA/PEDOT:PSS. Upon increasing the PEDOT:PSS concentration, the characteristic Raman band intensity of 4-MBA was enhanced. In addition, the selected b_2 vibration mode was significantly enhanced due to the influence of the charge transfer (CT) mechanism. The CT degree (ρ_{CT}) of the composite system was calculated before and after doping with PEDOT:PSS; when the concentration of PEDOT:PSS was 0.8%, the SERS intensity tended to be stable, and ρ_{CT} reached a maximum. Compared with that of the undoped PEDOT:PSS system, ρ_{CT} was significantly enhanced after doping, which can be explained by the CT effect induced by hydrogen bonds. These results indicate that hydrogen bonding transfers a charge from the Fermi energy level of Ag to the lowest unoccupied molecular orbital (LUMO) of 4-MBA, and due to the resulting potential difference, the charge will continue to transfer to the LUMO of PEDOT:PSS. Therefore, the introduction of organic semiconductors into the field of SERS not only expands the SERS substrate scope, but also provides a new idea for exploring the SERS mechanism. In addition, the introduction of hydrogen bonds has become an important guide for the study of CT and the structure of composite systems.

Keywords: surface-enhanced Raman scattering (SERS); charge transfer (CT); intermolecular hydrogen bonding; organic semiconductors



Citation: Pan, Y.; Wang, W.; Guo, S.; Jin, S.; Park, E.; Sun, Y.; Chen, L.; Jung, Y.M. Charge Transfer on the Surface-Enhanced Raman Scattering of Ag/4-MBA/PEDOT:PSS System: Intermolecular Hydrogen Bonding. *Chemosensors* **2021**, *9*, 111. <https://doi.org/10.3390/chemosensors9050111>

Academic Editor: Marco Pisco

Received: 14 April 2021

Accepted: 14 May 2021

Published: 17 May 2021

Publisher's Note: MDPI stays neutral with regard to jurisdictional claims in published maps and institutional affiliations.



Copyright: © 2021 by the authors. Licensee MDPI, Basel, Switzerland. This article is an open access article distributed under the terms and conditions of the Creative Commons Attribution (CC BY) license (<https://creativecommons.org/licenses/by/4.0/>).

1. Introduction

Surface-enhanced Raman scattering (SERS) is a fast and nondestructive method with the advantages of high sensitivity, good selectivity, high accuracy, and fast response. It is extensively used in various fields for research on detection, environmental pollution, food safety [1,2], homeland security [3], and chemical reaction mechanisms. Although SERS has been the subject of considerable interest and has been extensively studied, there are still minor issues that have been neglected. These issues are due to the sensitivity of SERS to the local environment of molecules and the influence of the local environment on the SERS distribution of adsorbates, including H^+ concentration, sensing, potential, and other factors [4,5]. In fact, there are many factors that affect the performance of SERS, such as intermolecular forces, which often affect the self-assembly process of polymer

molecules and liquid crystal molecules. By exploring intermolecular forces, we can better understand the properties of SERS and its influence on materials, allowing us to improve the properties of materials and broaden the substrate scope of SERS. Intermolecular forces usually include electrostatic interactions, van der Waals forces, dipole interactions, dispersion forces, and hydrogen bonding. Among them, the electrostatic effect was mainly affected by gravity or repulsion through positive and negative charges, affecting the SERS performance. Van der Waals forces hold matter together due to the asymmetric effects of electron clouds. Although the dipole-dipole interaction is weak, a large dipole moment still has a strong influence on the system. Dispersion force is the weakest intermolecular force, such as two molecules for the relative molecular mass of the material, and produces strong attraction. In particular, the study of hydrogen bonds, a kind of intermolecular force, provides some information on the internal structure of a molecule and interactions with other substances at the molecular level. Hydrogen bonding plays an important role in the study of molecular configuration, the identification of halogen bonding and the theoretical study of the transition from ground state to an excited state of a large number of chemicals and biological complex systems. Hydrogen bonds change the electronic structure of the nanocomposite system through the interaction between molecules, and then affects the SERS charge transfer process. Hydrogen bonds have been widely studied in recent years due to their directivity and saturation, which is very significant to the study of molecular structure and properties. We combined the research on hydrogen bonds with SERS according to the development status of SERS. Thus, the concentration-dependent Ag/4-MBA/PEDOT:PSS nanocomposite system was developed; however, the effect of hydrogen bonding on metal/semiconductor-molecule systems is still unclear and needs to be further improved. Therefore, studying hydrogen bonds via the SERS method can provide a better understanding of the SERS enhancement mechanism and allow further development of research on materials, chemical mechanisms, and environmental monitoring, biosensors, as well as research into other interdisciplinary fields.

The SERS enhancement mechanism is generally classified into two types: a chemical enhancement mechanism (CM) and an electromagnetic enhancement mechanism (EM). In the EM, the localized surface plasmon resonance (LSPR) excited by the rough surface of metal materials or the nanosized surface of a metal generates a strong electromagnetic field, resulting in Raman signal enhancement [6–8], and in the CM, an interaction between the target molecule and a metal surface forms a chemical bond, which enhances the SERS signal [9,10]. Among these mechanisms, the EM, which is a pure physical mechanism with a long-range effect that can produce a strong SERS signal without direct contact with a metal, is dominant. However, many phenomena in the experiment could not be fully explained by the electromagnetic field mechanism. For example, the distance between two nanoparticles (NPs) was not in the range of “hot spot”. Besides, different molecules had different SERS enhancement effects on the same SERS substrate. In this case, the CM could make up for the deficiency of the EM. Unlike the enhancement mechanism of electromagnetic field, CM is a short-range effect with a “first-layer effect”; that is, it can only enhance molecules restricted in monolayer by surface adsorption and bonding [11,12], and requires direct contact with metal NPs. The charge transfer (CT) model is a widely accepted CM model. CT is closely related to the mutual effect between molecules attached to the surface of a composite system and atoms attached to the surface of a composite system. When the incident light distribution matches the potential barrier between the Fermi energy level of the metal and the electron affinity energy of a molecule [13], it will induce a better CT effect, which is mainly attributed to the electron resonance process and the CT between the empty orbital of the molecule and the Fermi energy level of the metal [14,15]. The EM and CM do not work alone. These two mechanisms often play a synergistic role, so it is of great significance to establish an integrated model of the two mechanisms to jointly explain the SERS phenomenon.

In recent years, the progress of SERS research has been closely related to the development of SERS-active substrates. To achieve an excellent SERS effect, substrates should be

continuously improved. A strong SERS signal was first observed on rough silver (Ag) electrode surface-adsorbed pyridine and subsequently on the surfaces of Au, Ag, Cu and other coinage metals [16–21]. Then, it was discovered that transition metals can also produce excellent SERS effects as substrates [22]. Semiconductors have a controllable conductivity, universal structure, easily controlled synthesis [23], stable exciton formation and molecular structures with effective CT characteristics [24,25] and are gradually being applied with the development of flexible devices, trace detection, solar cells, and other new energy fields. In particular, organic semiconductors have been developed rapidly in recent years because they have the advantages of low cost, easy availability, good flexibility, few impurities, easy doping, energy level separation and recyclability.

Herein, a sandwich-structured noble metal-probe molecule-organic semiconductor was constructed via layer-by-layer assembly. Based on a study of the chain structure changes of PEDOT at different concentrations, the CT process was confirmed. We studied the SERS spectra of 4-mercaptobenzoic acid (4-MBA) induced by CT in different systems containing hydrogen bonding. Considering the influence of the CT degree (ρ_{CT}) on SERS intensity, we established a CT model, discussed the mechanism of CT, and further explained the role of hydrogen bonds. Therefore, the CT process between organic semiconductors and noble metals was explored to improve the theory that the CT process is an important factor to realize SERS enhancement.

2. Materials and Methods

2.1. Chemicals

PEDOT:PSS (1.5% in water) was obtained from Heraeus. Poly(diallyldimethylammonium chloride) (PDDA, numerator weight = 220,000–300,000, 20% in water) was obtained from J&K Chemical Co. 4-MBA (99%) and silver nitrate (AgNO_3 , 99.6%) was purchased from Sigma-Aldrich Co., Ltd. All the chemicals used in this study were purchased with the highest purity available and were used as received without further purification. Anhydrous ethanol (99.7%), hydrogen peroxide (H_2O_2 , 30%), ammonia (NH_3 , 28%) and deionized water (18.25 $\text{M}\Omega\cdot\text{cm}$) were also used throughout this study.

2.2. Preparation of Ag/4-MBA/ PEDOT:PSS Composites

2.2.1. Synthesis of Ag NPs

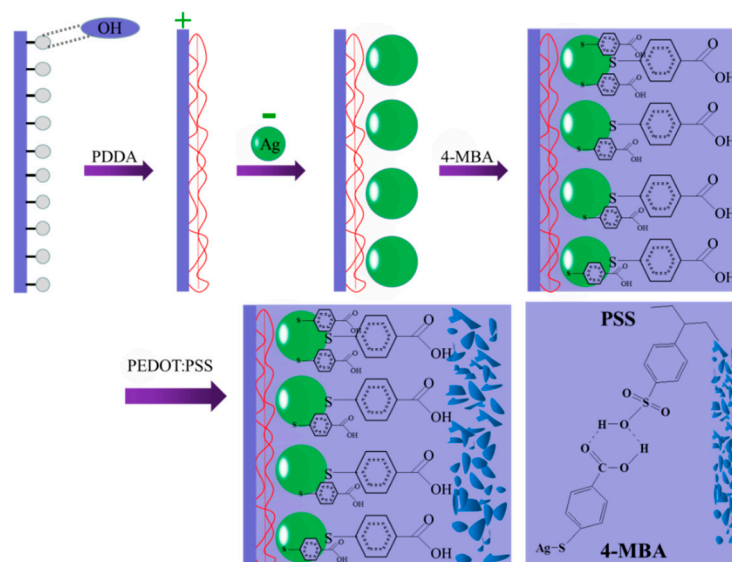
Ag NPs were prepared by the classic Lee method [26]. First, 0.036 g AgNO_3 was dissolved in 200 mL deionized water, and then the solution was stirred under reflux and heated to 90 °C. When the solution boiled slightly, 4 mL of 1% sodium citrate was added immediately, and the solution was heated to 85 °C for 45 min. During this process, the solution changed from colorless to light yellow, to brown, and finally, to a gray-green colloid with a maximum plasma absorption at approximately 430 nm. Ag NPs are spherical in distribution, and the average particle size was approximately 65 nm. A cleaned glass slide was placed in a mixed solution of H_2O , 30% H_2O_2 and 28% $\text{NH}_3\cdot\text{H}_2\text{O}$ (28% NH_3 in H_2O) at a volume ratio of 5:1:1. The solution was boiled until no bubbles were present and then cooled to room temperature, and the glass slide was washed several times with deionized water. A hydrophilic glass substrate rich in hydroxyl groups on the surface was obtained. The glass slide was immersed in 0.5% PDDA solution for 45 min, rinsed with deionized water, and allowed to dry naturally. The glass slide decorated with PDDA was soaked in a Ag sol for 8 h. Ag NPs were combined with the modified PDDA glass slide through electrostatic interaction, thereby obtaining Ag nanofilms with better particle dispersion.

2.2.2. Preparation of Ag/4-MBA System

Ag NPs were placed in a 4-MBA solution at a concentration of 10^{-3} M for 1 h, and the 4-MBA molecules were bonded to the surface of Ag NPs by Ag-S covalent bonds to complete the assembly of the Ag/4-MBA system.

2.2.3. PEDOT:PSS Deposition Procedure on the Ag/4-MBA System

Different concentrations of PEDOT:PSS (0.05%, 0.075%, 0.1%, 0.2%, 0.3%, 0.5%, 0.8%, and 1.0%) were dropped on the Ag/4-MBA-coated glass slide by titration method, and then naturally dried to complete the assembly, as shown in Scheme 1.



Scheme 1. Schematic of the layer-by-layer assembly of Ag/4-MBA/PEDOT:PSS films.

2.3. Characterization and SERS Measurements

The appearance and particle diameter of Ag NPs were determined by scanning electron microscopy (SEM) at a 250 kV accelerating voltage with a JEOL 6500 F microscope. A Shimadzu UV-3600 Plus UV-Vis spectrometer was used to measure the UV-Vis absorption spectra of the Ag/4-MBA and Ag/4-MBA/PEDOT:PSS composite systems. Raman spectra of the composite systems were obtained with a 633 nm laser by using a Renishaw Raman system 2000 microscope. For the Raman experiments of the Ag/4-MBA/PEDOT:PSS composite system, different concentrations (0.05%, 0.075%, 0.1%, 0.2%, 0.3%, 0.5%, 0.8%, and 1.0%) of PEDOT:PSS were titrated into the Ag/4-MBA composite system to form Ag/4-MBA/PEDOT:PSS systems.

3. Results

As shown in Scheme 1, first, the glass slide was coated with a positively charged polymer, PDDA. Second, the citrate ions stabilized Ag NPs was modified on the PDDA-coated glass slides based on the electrostatic adsorption interaction to form self-assembled Ag films. Third, 4-MBA was adsorbed on the Ag film to form the Ag/4-MBA system via Ag-S bonds. Finally, the Ag/4-MBA/PEDOT:PSS sandwich structure was formed by introducing the PEDOT:PSS to the Ag/4-MBA system via a hydrogen bond. Since the hydrogen is the electron acceptor, and oxygen is the electron donor, it is easy to form the hydrogen bond between the carboxyl of MBA and PEDOT or/and PSS. Herein, the oxygen on the carboxyl double bond of 4-MBA forms hydrogen bond with hydrogen on the sulfonic group of PSS, and the hydrogen on the carboxyl group of 4-MBA forms a hydrogen bond with oxygen on the sulfonic group [27]. Figure 1 displays SEM images of Ag NPs assembled on a PDDA-modified glass substrate and a Ag NP assembly system with different concentrations of PEDOT:PSS. According to the statistical distribution of particle size of Ag NPs in Figure 2, we found that most particle sizes of Ag NPs was obtained about 60–70 nm. As shown in Figure 1, before the introduction of PEDOT:PSS, Ag NPs were spherical distributed on the surface of glass substrate. After PEDOT:PSS coating, the morphology of Ag NPs self-assemble film was aggregated, and the aggregation degree increased gradually with the increase of the PEDOT:PSS.

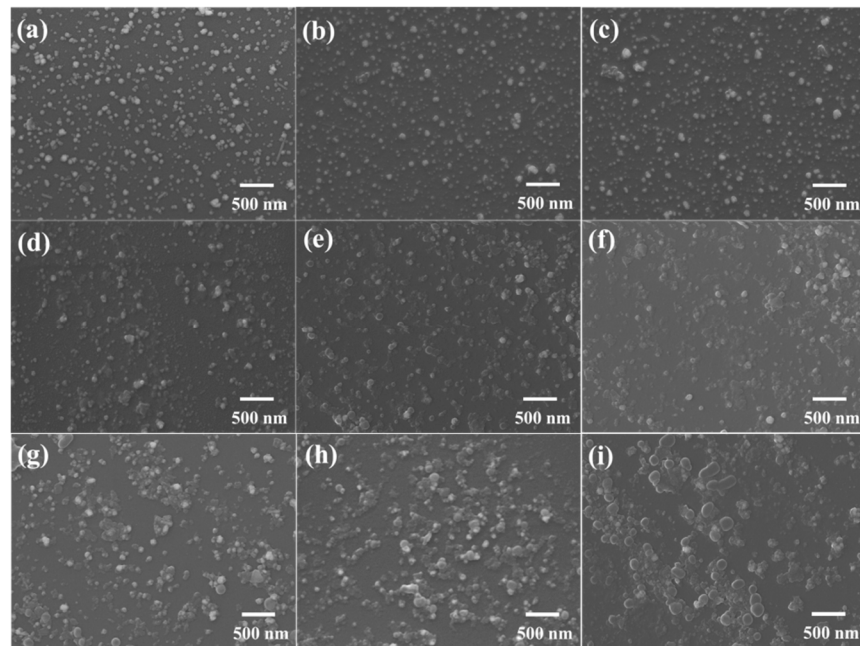


Figure 1. SEM images of (a) Ag NPs and (b–i) Ag/4-MBA/PEDOT:PSS (the concentrations were 0.05%, 0.075%, 0.1%, 0.2%, 0.3%, 0.5%, 0.8%, and 1.0%).

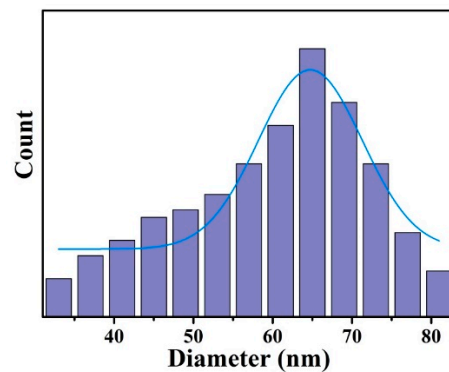


Figure 2. The statistical distribution of particle size of Ag NPs.

The compositions, contents and structures of different systems can be determined and analyzed by UV-Vis spectroscopy. Figure 3 shows the UV-Vis absorption spectra of Ag NPs, Ag/4-MBA, and Ag/4-MBA/PEDOT:PSS composite systems (PEDOT:PSS concentrations were 0.05%, 0.075%, 0.1%, 0.2%, 0.3%, 0.5%, 0.8%, and 1.0%, respectively). The Ag NPs were deposited on the PDPA-decorated glass slide by employing the self-assemble method. After deposition of the Ag NPs on the PDPA-decorated glass slide, the distance of Ag NPs decreased and the aggregation occurred, which induced wide absorbance bands located at 400–700 nm. The strong interactions and coupling may have also contributed to the plasmon resonance red shift if the LSPR existed between neighboring Ag NPs. The dipole–dipole interaction assigned to Ag NP were blue shifted by 22 nm more than the silver sol. After different concentrations of PEDOT:PSS were added, the SPR peak of Ag NPs continued to shift to longer wavelengths, and as the concentration increased, the redshift phenomenon became more obvious, and the peak gradually widened. After introduction of the polymer, layers of Ag, 4-MBA and PEDOT:PSS interacted to form a new CT state [28].

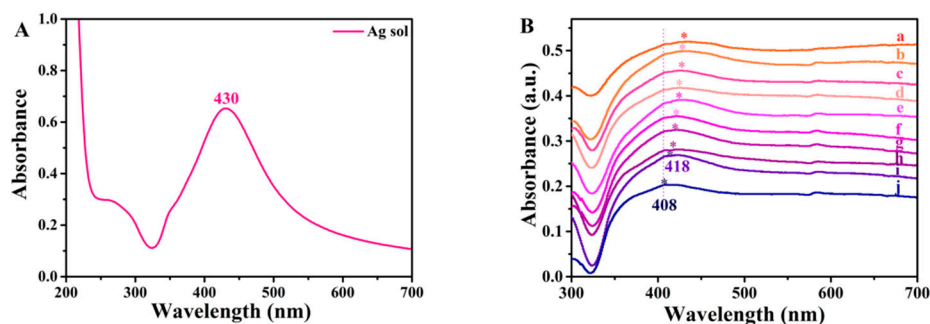


Figure 3. (A) UV-Vis absorption spectra of Ag sol, (B) Ag/4-MBA/PEDOT:PSS ((a) 1.0%, (b) 0.8%, (c) 0.5%, (d) 0.3%, (e) 0.2%, (f) 0.1%, (g) 0.075%, and (h) 0.05%, (i) Ag/4-MBA and (j) Ag NPs) composite systems.

Figure 4 shows the Raman spectrum of 4-MBA with 633 nm laser excitation. The band assignment of 4-MBA in the Ag/4-MBA/PEDOT:PSS system is shown in Table 1. In the SERS (Figure 5A) of the Ag/4-MBA/PEDOT:PSS composite complex system with different concentrations of PEDOT:PSS, bands at 1263 ($\nu_{C\alpha-C\alpha}$ inter-ring), 1395 ($\nu_{C\beta-C\beta}$ inter-ring) and 1484 ($\nu_{sym}C\alpha=C\beta$) cm^{-1} were observed. The bands assigned to PEDOT:PSS and 4-MBA are marked with circles and squares, respectively. With increasing PEDOT:PSS concentration, the overall intensity of the SERS bands corresponding to 4-MBA increased gradually. When the concentration of PEDOT:PSS was 0.8%, the intensity change became stable. Due to the formation of the hydrogen bond between PEDOT:PSS and 4-MBA the electron cloud density of 4-MBA was changed [29–31]. In turn, it affected the electronic structure of the Ag/4-MBA complex, and the intensity of the 4-MBA band also changed. With increasing PEDOT:PSS concentration, the number of carboxyl groups combined with PSS increased, and the effect on the system increased. When the concentration of PEDOT:PSS increased to a certain extent, the number of carboxyl groups bound to PSS in the system became saturated, and the influence on the system became stable [32]. For comparison, SERS spectra of Ag/4-MBA/0.8% PEDOT:PSS, Ag/4-MBA, Ag/0.8% PEDOT:PSS, 4-MBA/0.8% PEDOT:PSS, and 0.8% PEDOT:PSS were shown in Figure 5B. Compared with the original 0.8% PEDOT:PSS system, the Ag/4-MBA/0.8% PEDOT:PSS composite system exhibited a larger blueshift at 1395–1437 cm^{-1} because Ag and sulfhydryl groups combined through Ag-S bonds to form a structure with C_{2v} symmetry. 4-MBA is a derivative containing sulfhydryl and carboxyl groups [33–36]. It has two hydrogen bond donors, namely, the oxygen atoms on the sulfhydryl and carboxyl groups, and five potential hydrogen bond acceptors, namely, π electrons on the benzene ring and the lone pair electrons of the oxygen and sulfur atoms.

Table 1. Band assignments for the spectrum of 4-MBA in the Ag/4-MBA/PEDOT:PSS composite system under 633 nm excitation.

Wavenumber (cm^{-1})	Band Assignments	Corresponding Molecule
1014	In-plane ring breathing, b_2	4-MBA
1077	In-plane ring breathing + $\nu(CS)$	4-MBA
1143	C-H deformation modes, b_2	4-MBA
1184	C-H deformation modes, a_1	4-MBA
1263	$\nu(C\alpha-C\alpha)$ inter-ring	PEDOT:PSS
1395	$\beta(O-H)$ + $\nu(C-ph)$ + in-plane $\nu(CC)$ + asymmetry $\alpha(CO_2)$, b_2 and $\nu(C\beta-C\beta')$ inter-ring	4-MBA and PEDOT:PSS
1437	$\nu_{sym}(C\alpha=C\beta)$	PEDOT:PSS
1484	$\nu_{sym}(C\alpha=C\beta)$	PEDOT:PSS
1589	Totally symmetric $\nu(CC)$, a_1	4-MBA
1712	C=O stretching	4-MBA

ν , stretching; β , bending. For ring vibrations, the corresponding vibrational mode of the benzene ring and the symmetry state under C_{2v} symmetry are proposed.

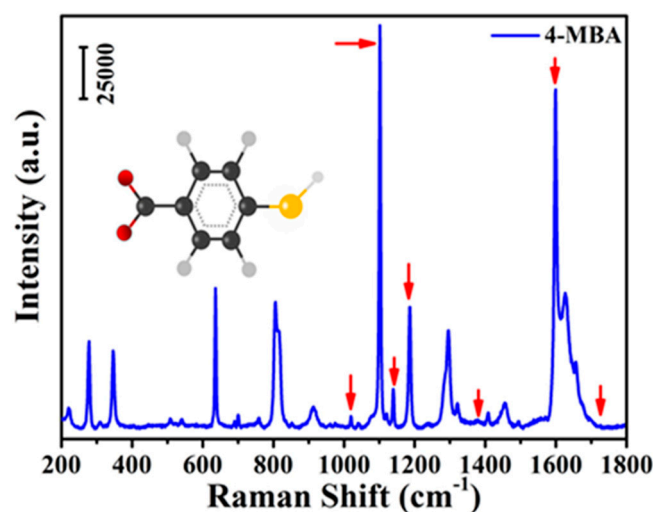


Figure 4. Raman spectra of 4-MBA powder under 633 nm excitation.

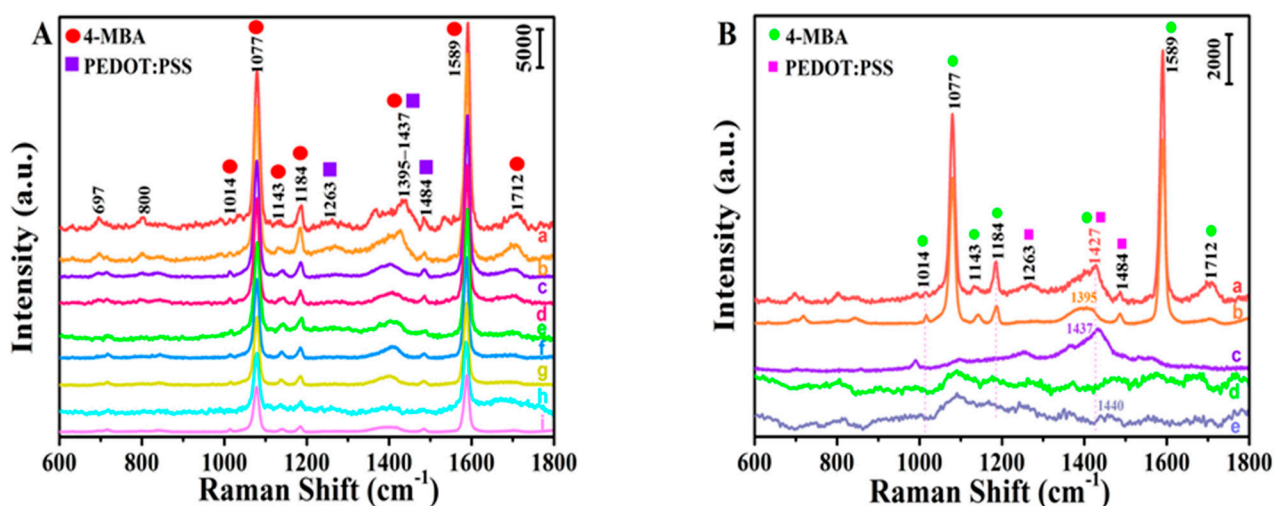


Figure 5. (A) SERS spectra of the Ag/4-MBA/PEDOT:PSS composite system with different concentrations of PEDOT:PSS (a–i: 1.0%, 0.8%, 0.5%, 0.3%, 0.2%, 0.1%, 0.075%, 0.05%, and 0%). (B) SERS spectra of (a) Ag/4-MBA/0.8% PEDOT:PSS, (b) Ag/4-MBA, (c) Ag/0.8% PEDOT:PSS, (d) 4-MBA/0.8% PEDOT:PSS, and (e) 0.8% PEDOT:PSS.

When PSS bound to 4-MBA, the three lone pairs of electrons on the oxygen atom of the sulfonic group of PSS served as donors, and the hydrogen on the carboxyl group of 4-MBA served as an acceptor. With the combination of the two forms of hydrogen bonds, the conjugation degree of the whole system increased, the density of the electron cloud increased, and the vibration signal shifted to higher wavenumbers, corresponding to a blueshift. This phenomenon shows that hydrogen bonding in the molecule led to charge redistribution of the Ag/4-MBA complex. According to the ρ_{CT} formula proposed by Lombardi, the contribution of the hydrogen bond to CT resonance was estimated [37,38].

The calculation formula is as follows [39]:

$$\rho_{CT}(\kappa) = \frac{I^k(CT) - I^k(SPR)}{I^k(CT) + I^0(SPR)} \quad (1)$$

The exponent k represents the line of the Raman spectrum when the molecule has CT resonance. When $I^0(SPR) = I^k(SPR)$, spectral line k belongs to a completely symmetric membrane, and when the $I^k(SPR)$ value is extremely small or close to 0, the SERS spectral

intensity mainly comes from the contribution of CT. The formula can be approximated as follows:

$$\rho_{CT}(\kappa) = \frac{I^k(CT)}{I^k(CT) + I^0(SPR)} \quad (2)$$

Here, the band at 1184 cm^{-1} attributed to C-H deformation mode (a_1 mode) and $1395\text{--}1437 \text{ cm}^{-1}$ (b_2 mode) were selected to calculate ρ_{CT} . The ρ_{CT} values of the Ag/4-MBA/PEDOT:PSS composite systems with different concentrations of PEDOT:PSS are shown in Table 2 and Figure 6A. This band corresponds to an in-plane circulatory breathing mode, which is coupled to the $\nu C\text{--}S$ circulatory breathing mode (b_2 mode) of 4-MBA at 1014 cm^{-1} . At present, it is only slightly affected by SPR, mainly due to the contribution of CT. By calculating the ρ_{CT} of 4-MBA and the ratio of b_2 to a_1 , the relationship between these values and the PEDOT:PSS concentration was obtained. When $\rho_{CT}(\kappa) = 0.5$, the contributions of SPR and CT to SERS enhancement were the same; when $\rho_{CT}(\kappa) = 0$, the mainly SPR effect affected SERS enhancement. When $\rho_{CT}(\kappa)$ was about 1, the mainly CT effect affected the SERS enhancement. As shown in Figure 6B, $\rho_{CT}(\kappa) = 0.395$ and 0.650 for the Ag/4-MBA composite system and Ag/4-MBA/PEDOT:PSS (0.8%) composite system, respectively. Therefore, for the Ag/4-MBA/PEDOT:PSS (0.8%) composite system, $\rho_{CT}(\kappa) > 0.5$ was due to the CT process of the system. Figure 6A shows a column chart of the ρ_{CT} values of the Ag/4-MBA/PEDOT:PSS composite system with different concentrations of PEDOT:PSS (0.05%, 0.075%, 0.1%, 0.2%, 0.3%, 0.5%, 0.8%, and 1.0%). There is a positive correlation between ρ_{CT} and PEDOT:PSS concentration, indicating that the formation of hydrogen bonds is beneficial to the CT process [40,41]. As the number of hydrogen bonds increased, the CT process of Ag/4-MBA was further distributed to form a CT state, forming a CT state more matched to the incident light. When the PEDOT:PSS concentration was 0.8%, the CT distribution was stable.

Table 2. ρ_{CT} values of Ag/4-MBA/PEDOT:PSS systems with different PEDOT:PSS concentrations.

Ag/4-MBA/PEDOT:PSS Composite Systems with Different Concentration of PEDOT:PSS	ρ_{CT}
0%	0.395
0.05%	0.540
0.075%	0.549
0.1%	0.560
0.2%	0.570
0.3%	0.579
0.5%	0.603
0.8%	0.650
1.0%	0.610

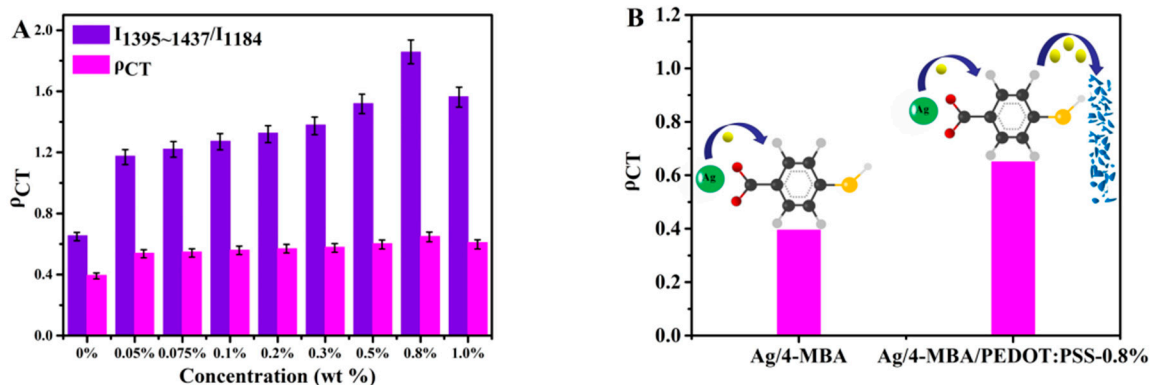


Figure 6. (A) Column chart of ρ_{CT} values of the Ag/4-MBA/PEDOT:PSS composite system with different concentrations of PEDOT:PSS (0%, 0.05%, 0.075%, 0.1%, 0.2%, 0.3%, 0.5%, 0.8%, and 1.0%). (B) Column chart of ρ_{CT} values of the Ag/4-MBA/PEDOT:PSS composite system (0.8% PEDOT:PSS) and Ag/4-MBA.

When Ag, 4-MBA and PEDOT:PSS contacted each other, a new CT process occurred at the contact interface, and a new CT state formed. The Fermi energy level of Ag NPs in vacuum is -4.84 eV [42], and the highest occupied molecular orbital (HOMO) and lowest unoccupied molecular orbital (LUMO) of 4-MBA have energies of -8.48 eV and -3.21 eV, respectively [43]. The HOMO and LUMO of PEDOT:PSS are -6.20 eV and -5.50 eV [44], respectively, and the band gap (E_g) is 1.80 eV. Figure 7 shows the CT process in the Ag/4-MBA/PEDOT:PSS composite system. Under 633 nm excitation, the incident light energy is 1.96 eV, the Fermi level of Ag is full of electrons, the electrons are excited to the LUMO level of the 4-MBA molecule, and the electrons will continue to transfer to the LUMO level of PEDOT:PSS because of the potential difference. An electron in the HOMO level of PEDOT:PSS is excited to the LUMO level of PEDOT:PSS and then transferred to the LUMO level of the 4-MBA molecule. When the LUMO level of PEDOT:PSS is full of electrons, the LUMO level of PEDOT:PSS will increase, while the Fermi energy level of Ag will decrease until the Fermi levels of both sides are equal. In this case, the CT velocity in both directions is equal, and the SERS signal is stable [45]. For the Ag/4-MBA system, $\rho_{CT}(\kappa)$ is 0.395 , which means that the EM is still dominant in the Ag/4-MBA system. By introducing PEDOT:PSS, the electron continues to transfer from the LUMO level of 4-MBA to the LUMO level of PEDOT:PSS, and the electron is excited from the HOMO level of PEDOT:PSS to the LUMO level of PEDOT:PSS and the LUMO level of 4-MBA, resulting in an increase in $\rho_{CT}(\kappa)$ from 0.395 to 0.650 , which indicates a new CT process. The CT process has considerable effects on SERS enhancement, thus increasing the SERS intensity. Compared with the Ag/4-MBA system, the Ag/4-MBA/PEDOT:PSS composite system exhibits better SERS activity because PEDOT:PSS increases the contributions of CT.

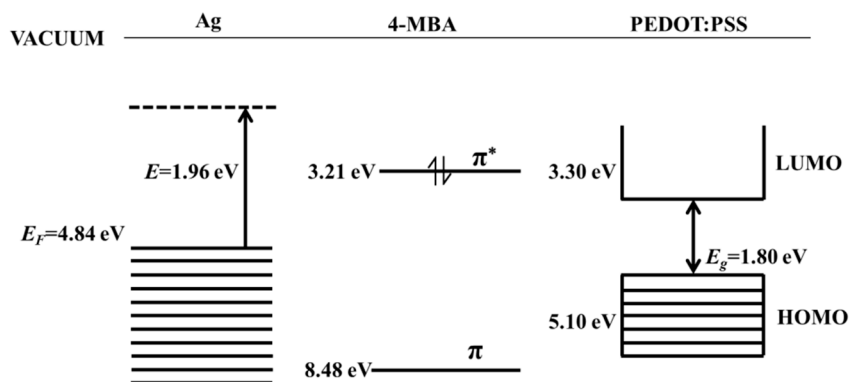


Figure 7. CT mechanism in terms of the Ag/4-MBA/PEDOT:PSS energy level diagram.

4. Conclusions

Ag/4-MBA/PEDOT:PSS composite systems with different concentrations of PEDOT:PSS (0, 0.05%, 0.075%, 0.1%, 0.2%, 0.3%, 0.5%, 0.8%, and 1.0%) were successfully constructed by the layer-by-layer assembly method. The hydrogen bonds between the probe molecule 4-MBA and the polymer PEDOT:PSS were studied by SERS. Ag/4-MBA/PEDOT:PSS composite systems with different concentrations of PEDOT:PSS were studied, and their ρ_{CT} values were calculated. When the PEDOT:PSS concentration was 0.8%, the intensity increase tended to be stable, and ρ_{CT} reached a maximum. Compared with that of the undoped system, the ρ_{CT} value of the doped system increased, which was attributed to the CT process. In terms of the mechanism, the formation of hydrogen bonds promotes charge excitation from the Fermi level of Ag to the LUMO level of the 4-MBA molecule, and the electrons will continue to transfer to the LUMO level of PEDOT:PSS under the action of a potential difference. This distinctly shows that the change in SERS intensity can be attributed to the molecular hydrogen bond formed by PEDOT:PSS and 4-MBA. The addition of organic semiconductors greatly improved the study of SERS and provided new ideas for research on flexible device development, biosensors, trace analysis, food safety, and environmental protection.

Author Contributions: Methodology, Y.P. and S.G.; software, W.W., S.J. and E.P.; formal analysis, Y.S. and L.C.; data curation, Y.P. and W.W.; writing—original draft preparation, Y.P., S.J. and E.P.; writing—review and editing, Y.S., L.C. and Y.M.J.; supervision, L.C. and Y.M.J.; project administration, Y.M.J. All authors have read and agreed to the published version of the manuscript.

Funding: This research was funded by Jilin Normal University (Jishi Scholar). This work was also supported by the National Research Foundation of Korea (NRF) grants funded by the Korea government (No. NRF-2021R1A2C2004550, No. NRF-2020K2A9A2A06036299 and No. NRF-2020R1A4A1016093).

Institutional Review Board Statement: Not applicable.

Informed Consent Statement: Not applicable.

Data Availability Statement: Do not have the supporting reported results.

Conflicts of Interest: The authors declare no conflict of interest.

References

1. Zheng, J.; He, L. Surface-enhanced Raman spectroscopy for the chemical analysis of food. *Compr. Rev. Food Sci. F* **2014**, *13*, 317–328. [[CrossRef](#)]
2. Yang, T.; Zhao, B.; Hou, R.; Zhang, Z.; Kinchla, A.J.; Clark, J.M.; He, L. Evaluation of the penetration of multiple classes of pesticides in fresh produce using surface-enhanced Raman scattering mapping. *J. Food. Sci.* **2016**, *81*, T2891–T2901. [[CrossRef](#)]
3. Lee, C.H.; Tian, L.; Singamaneni, S. Paper-based SERS swab for rapid trace detection on real-world surfaces. *ACS Appl. Mater. Interfaces* **2010**, *2*, 3429–3435. [[CrossRef](#)] [[PubMed](#)]
4. Hu, J.W.; Zhao, B.; Xu, W.Q.; Li, B.F.; Fan, Y.G. Surface-enhanced Raman spectroscopy study on the structure changes of 4-mercaptopyridine adsorbed on silver substrates and silver colloids. *Spectrochim. Acta A* **2002**, *58*, 2827–2834. [[CrossRef](#)]
5. Kim, K.; Kim, K.L.; Choi, J.Y.; Shin, D.; Shin, K.S. Effect of volatile organic chemicals on surface-enhanced Raman scattering of 4-aminobenzenethiol on Ag: Comparison with the potential dependence. *Phys. Chem. Chem. Phys.* **2011**, *13*, 15603–15609. [[CrossRef](#)] [[PubMed](#)]
6. Langhammer, C.; Yuan, Z.; Zoric, I.; Kasemo, B. Plasmonic properties of supported Pt and Pd nanostructures. *Nano Lett.* **2006**, *6*, 833–838. [[CrossRef](#)] [[PubMed](#)]
7. Zhang, W.; Cui, X.; Yeo, B.-S.; Schmid, T.; Hafner, C.; Zenobi, R. Nanoscale roughness on metal surfaces can increase tip-enhanced Raman scattering by an order of magnitude. *Nano Lett.* **2007**, *7*, 1401–1405. [[CrossRef](#)]
8. Popp, J.; Mayerhoefer, T. Surface-enhanced Raman spectroscopy. *Anal. Bioanal. Chem.* **2009**, *394*, 1717–1718. [[CrossRef](#)]
9. Champion, A.; Kambhampati, P. Surface-enhanced Raman scattering. *Chem. Soc. Rev.* **1998**, *27*, 241–250. [[CrossRef](#)]
10. Haynes, C.L.; McFarland, A.D.; Van Duyne, R.P. Surface-enhanced Raman spectroscopy. *Anal. Chem.* **2005**, *77*, 338A–346A. [[CrossRef](#)]
11. Otto, A. The ‘chemical’ (electronic) contribution to surface-enhanced Raman scattering. *J. Raman Spectrosc.* **2005**, *36*, 497–509. [[CrossRef](#)]
12. Dresselhaus, M.S.; Jorio, A.; Hofmann, M.; Dresselhaus, G.; Saito, R. Perspectives on carbon nanotubes and graphene Raman spectroscopy. *Nano Lett.* **2010**, *10*, 751–758. [[CrossRef](#)] [[PubMed](#)]
13. Fateixa, S.; Nogueira, H.I.S.; Trindade, T. Hybrid nanostructures for SERS: Materials development and chemical detection. *Phys. Chem. Chem. Phys.* **2015**, *17*, 21046–21071. [[CrossRef](#)] [[PubMed](#)]
14. Lombardi, J.R.; Birke, R.L. A unified approach to surface-enhanced Raman spectroscopy. *J. Phys. Chem. C* **2008**, *12*, 5605–5617. [[CrossRef](#)]
15. Sun, M.T.; Fang, Y.R.; Yang, Z.L.; Xu, H.X. Chemical and electromagnetic mechanisms of tip-enhanced Raman scattering. *Phys. Chem. Chem. Phys.* **2009**, *11*, 9412–9419. [[CrossRef](#)]
16. Hu, X.; Meng, G.; Huang, Q.; Xu, W.; Han, F.; Sun, K.; Xu, Q.; Wang, Z. Large-scale homogeneously distributed Ag-NPs with sub-10 nm gaps assembled on a two-layered honeycomb-like TiO₂ film as sensitive and reproducible SERS substrates. *Nanotechnology* **2012**, *23*, 385705. [[CrossRef](#)]
17. Kneipp, K.; Wang, Y.; Kneipp, H.; Perelman, L.T.; Itzkan, I.; Dasari, R.; Feld, M.S. Single molecule detection using surface-enhanced Raman scattering (SERS). *Phys. Rev. Lett.* **1997**, *78*, 1667–1670. [[CrossRef](#)]
18. Dieringer, J.A.; McFarland, A.D.; Shah, N.C.; Stuart, D.A.; Whitney, A.V.; Yonzon, C.R.; Young, M.A.; Zhang, X.Y.; Van Duyne, R.P. Surface enhanced Raman spectroscopy: New materials, concepts, characterization tools, and applications. *Faraday Discuss.* **2006**, *132*, 9–26. [[CrossRef](#)]
19. Whitney, A.V.; Myers, B.D.; Van Duyne, R.P. Sub-100 nm triangular nanopores fabricated with the reactive ion etching variant of nanosphere lithography and angle-resolved nanosphere lithography. *Nano Lett.* **2004**, *4*, 1507–1511. [[CrossRef](#)]
20. Ren, B.; Lin, X.F.; Yang, Z.L.; Liu, G.K.; Aroca, R.F.; Mao, B.W.; Tian, Z.Q. Surface-enhanced Raman scattering in the ultraviolet spectral region: UV-SERS on rhodium and ruthenium electrodes. *J. Am. Chem. Soc.* **2003**, *125*, 9598–9599. [[CrossRef](#)]
21. Yoshida, K.; Itoh, T.; Biju, V.; Ishikawa, M.; Ozaki, Y. Spectral shapes of surface-enhanced resonance Raman scattering sensitive to the refractive index of media around single Ag nanoaggregates. *Appl. Phys. Lett.* **2009**, *95*, 263104. [[CrossRef](#)]

22. Tian, Z.Q.; Ren, B.; Wu, D.Y. Surface-enhanced Raman scattering: From noble to transition metals and from rough surfaces to ordered nanostructures. *J. Phys. Chem. B* **2002**, *106*, 9463–9483. [[CrossRef](#)]
23. Yilmaz, M.; Babur, E.; Ozdemir, M.; Giesecking, R.L.; Dede, Y.; Tamer, U.; Schatz, G.C.; Facchetti, A.; Usta, H.; Demirel, G. Nanostructured organic semiconductor films for molecular detection with surface-enhanced Raman spectroscopy. *Nat. Mater.* **2017**, *16*, 918. [[CrossRef](#)] [[PubMed](#)]
24. Demirel, G.; Usta, H.; Yilmaz, M.; Celik, M.; Alidagi, H.A.; Buyukserin, F. Surface-enhanced Raman spectroscopy (SERS): An adventure from plasmonic metals to organic semiconductors as SERS platforms. *J. Mater. Chem. C* **2018**, *6*, 5314–5335. [[CrossRef](#)]
25. Sharma, B.; Frontiera, R.R.; Henry, A.I.; Ringe, E.; Van Duyne, R.P. SERS: Materials, applications, and the future. *Mater. Today* **2012**, *15*, 16–25. [[CrossRef](#)]
26. Lee, P.C.; Meisel, D. Adsorption And Surface-Enhanced Raman of Dyes on Silver and Gold Sols. *J. Phys. Chem.* **1982**, *86*, 3391–3395. [[CrossRef](#)]
27. Liang, Z.; Mao, Q.; Wang, Y.-P.; Zhu, F.-C.; Li, J.-X.; Yao, X.; Gao, F.; Wu, X.; Xu, M.; Wang, J.-Z. Progress on the research and development of inactivated EV71 whole-virus vaccines. *Hum. Vaccin. Immunother.* **2013**, *9*, 1701–1705. [[CrossRef](#)] [[PubMed](#)]
28. Mulvaney, P. Surface plasmon spectroscopy of nanosized metal particles. *Langmuir* **1996**, *12*, 788–800. [[CrossRef](#)]
29. Nakamura, H. Roles of electrostatic interaction in proteins. *Q. Rev. Biophys.* **1996**, *29*, 1–90. [[CrossRef](#)]
30. Ye, A.Q. Complexation between milk proteins and polysaccharides via electrostatic interaction: Principles and applications—A review. *Int. J. Food. Sci. Tech.* **2008**, *43*, 406–415. [[CrossRef](#)]
31. Kolny, J.; Kornowski, A.; Weller, H. Self-organization of cadmium sulfide and gold nanoparticles by electrostatic interaction. *Nano Lett.* **2002**, *2*, 361–364. [[CrossRef](#)]
32. Demirel, G.; Giesecking, R.L.M.; Ozdemir, R.; Kahmann, S.; Loi, M.A.; Schatz, G.C.; Facchetti, A.; Usta, H. Molecular engineering of organic semiconductors enables noble metal-comparable SERS enhancement and sensitivity. *Nat. Commun.* **2019**, *10*, 9. [[CrossRef](#)]
33. Bishnoi, S.W.; Rozell, C.J.; Levin, C.S.; Gheith, M.K.; Johnson, B.R.; Johnson, D.H.; Halas, N.J. All-optical nanoscale pH meter. *Nano Lett.* **2006**, *6*, 1687–1692. [[CrossRef](#)] [[PubMed](#)]
34. Lee, S.J.; Moskovits, M. Visualizing chromatographic separation of metal ions on a surface-enhanced Raman active medium. *Nano Lett.* **2011**, *1*, 145–150. [[CrossRef](#)]
35. Scaffidi, J.P.; Gregas, M.K.; Seewaldt, V.; Vo-Dinh, T. SERS-based plasmonic nanobiosensing in single living cells. *Anal. Bioanal. Chem.* **2009**, *393*, 1135–1141. [[CrossRef](#)]
36. Tan, E.Z.; Yin, P.G.; You, T.T.; Wang, H.; Guo, L. Three dimensional design of large-scale TiO₂ nanorods scaffold decorated by silver nanoparticles as SERS sensor for ultrasensitive malachite green detection. *ACS Appl. Mater. Interfaces* **2012**, *4*, 3432–3437. [[CrossRef](#)]
37. Levitt, M.; Perutz, M.F. Aromatic rings act as hydrogen-bond acceptors. *J. Mol. Biol.* **1988**, *201*, 751–754. [[CrossRef](#)]
38. Bell, D.A.; Anslyn, E.V. Complexation of carbonyl-compounds with an organic salt dominated by acid-base interactions in dichloromethane. *J. Org. Chem.* **1994**, *59*, 512–514. [[CrossRef](#)]
39. Lombardi, J.R.; Birke, R.L. A unified view of surface-enhanced Raman scattering. *Acc. Chem. Res.* **2009**, *42*, 734–742. [[CrossRef](#)]
40. Ratajczak, H.; Orville, W.J. Charge-transfer properties of hydrogen-bond 0.6. charge-transfer theory and dipole-moments of hydrogen-bonded complexes. *J. Mol. Struct.* **1975**, *26*, 387–391. [[CrossRef](#)]
41. Ratajczak, H.; Orville, W.J. Charge-transfer properties of hydrogen-bonds 0.3. charge-transfer theory and relation between energy and enhancement of dipole-moment of hydrogen-bonded complexes. *J. Chem. Phys.* **1973**, *58*, 911–919. [[CrossRef](#)]
42. Zhang, X.L.; Yu, Z.; Ji, W.; Sui, H.M.; Gong, Q.; Wang, X.; Zhao, B. Charge-transfer effect on surface-enhanced Raman scattering (SERS) in an ordered Ag NPs/4-mercaptobenzoic acid/TiO₂ system. *J. Phys. Chem. C* **2015**, *119*, 22439–22444. [[CrossRef](#)]
43. Chen, L.; Zhang, F.; Deng, X.Y.; Xue, X.X.; Wang, L.; Sun, Y.T.; Feng, J.D.; Zhang, Y.J.; Wang, Y.X.; Jung, Y.M. SERS study of surface plasmon resonance induced carrier movement in Au@Cu₂O core-shell nanoparticles. *Spectrochim. Acta A* **2018**, *189*, 608–612. [[CrossRef](#)] [[PubMed](#)]
44. Iwan, A.; Caballero-Briones, F.; Filapek, M.; Boharewicz, B.; Tazbir, I.; Hreniak, A.; Guerrero-Contreras, J. Electrochemical and photocurrent characterization of polymer solar cells with improved performance after GO addition to the PEDOT:PSS hole transporting layer. *Sol. Energy* **2017**, *146*, 230–242. [[CrossRef](#)]
45. Wu, X.J.; Li, Q.X.; Huang, J.; Yang, J.L. Nonequilibrium electronic transport of 4,4'-bipyridine molecular junction. *J. Chem. Phys.* **2015**, *123*, 184712. [[CrossRef](#)]